

## Supporting Information

### **Efficient Electrosynthesis of Urea Using CO<sub>2</sub> and Nitrate over a Bifunctional In<sub>4</sub>SnS<sub>8</sub> Catalyst**

Mao Li,<sup>a</sup> Yanan Gao,<sup>\*a</sup> Ji Xu,<sup>a</sup> Sangzi Wang,<sup>a</sup> Yujin Wei,<sup>a</sup> Jingru Wang,<sup>a</sup> Bo Ouyang,<sup>\*b</sup> Kun Xu<sup>\*a</sup>

<sup>a</sup> School of Chemistry and Chemical Engineering, Key Laboratory of Functional Inorganic Material Chemistry of Anhui Province, Anhui Province Key Laboratory of Chemistry for Inorganic/Organic Hybrid Functionalized Materials, Key Laboratory of Structure and Functional Regulation of Hybrid Materials of Ministry of Education, Anhui University, Hefei 230601, China. \*Email: gaoyanan@ahu.edu.cn; kunxu@ahu.edu.cn

<sup>b</sup> MIIT Key Laboratory of Semiconductor Microstructure and Quantum Sensing, School of Science, Nanjing University of Science and Technology, Nanjing 210094, China. \*Email: ouyangboyi@njust.edu.cn

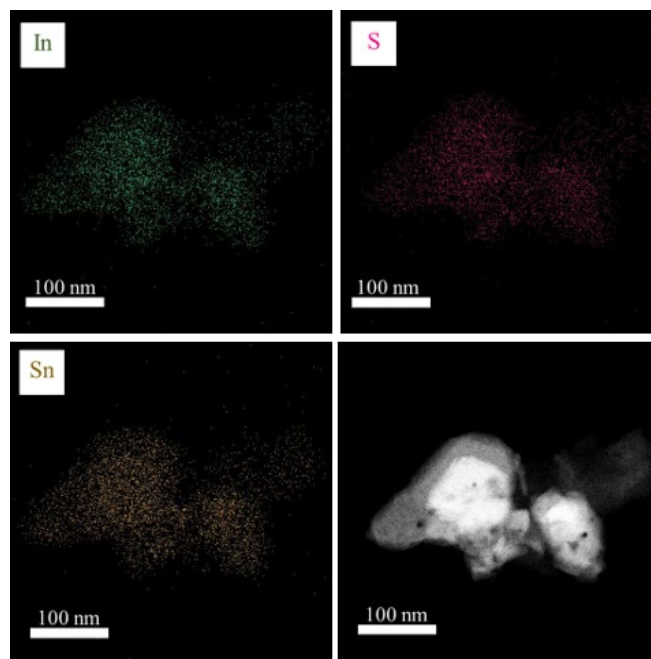


**Fig. S1** Element mapping of  $\text{In}_4\text{SnS}_8$ .

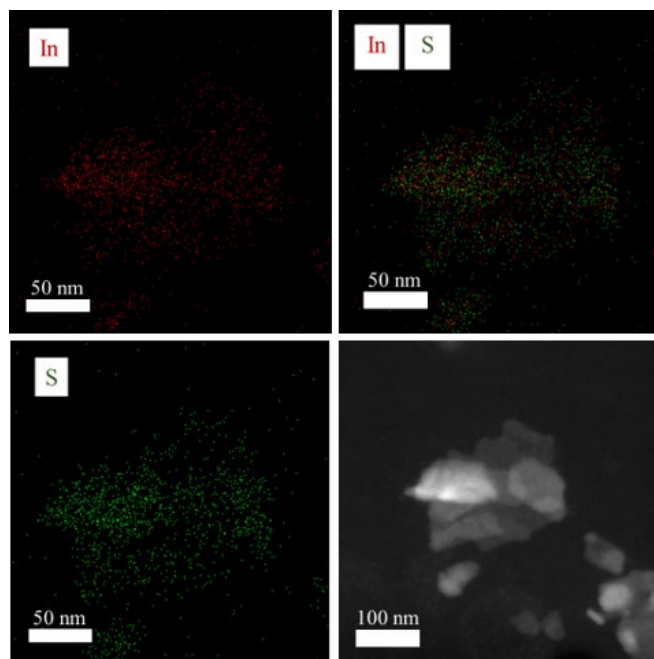


**Fig. S2** Element mapping of  $\text{In}_2\text{S}_3$ .

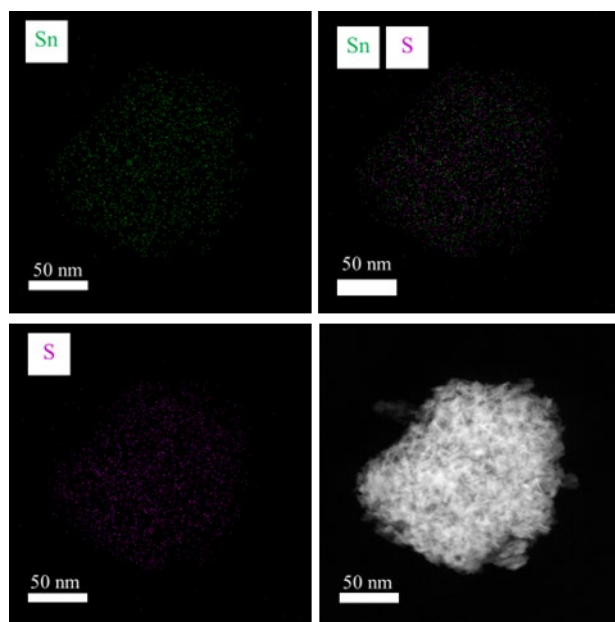


**Fig. S3** Element mapping of SnS<sub>2</sub>.

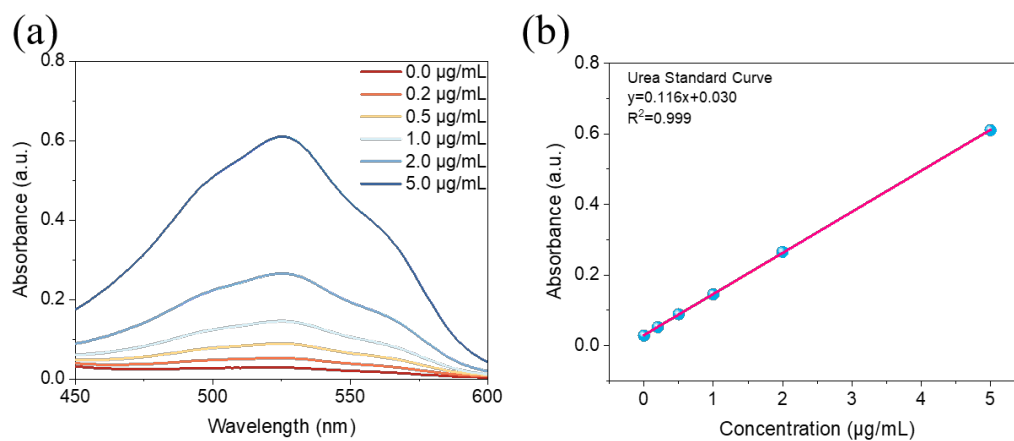


**Fig. S4** (a) UV-Vis absorption spectra of urea standard solutions with different concentrations. (b) Calibration curve for quantitative analysis of urea concentration.

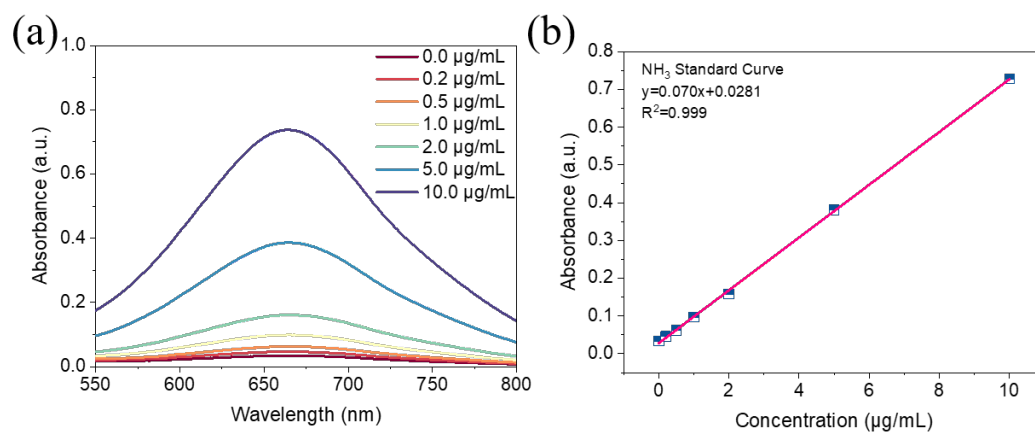


**Fig. S5** (a) UV-Vis absorption spectra of  $\text{NH}_3$  standard solutions with different concentrations. (b) Calibration curve for quantitative analysis of  $\text{NH}_3$  concentration.

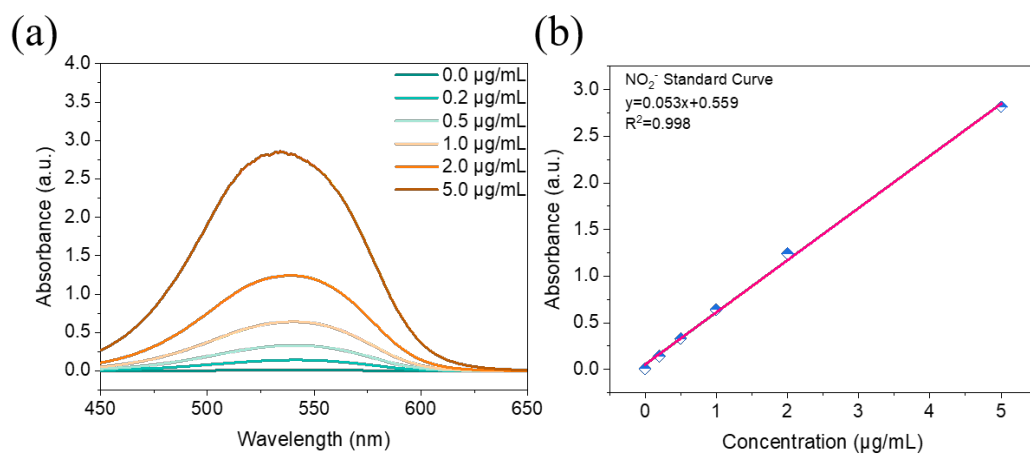


**Fig. S6** (a) UV-Vis absorption spectra of  $\text{NO}_2^-$  standard solutions with different concentrations. (b) Calibration curve for quantitative analysis of  $\text{NO}_2^-$  concentration.

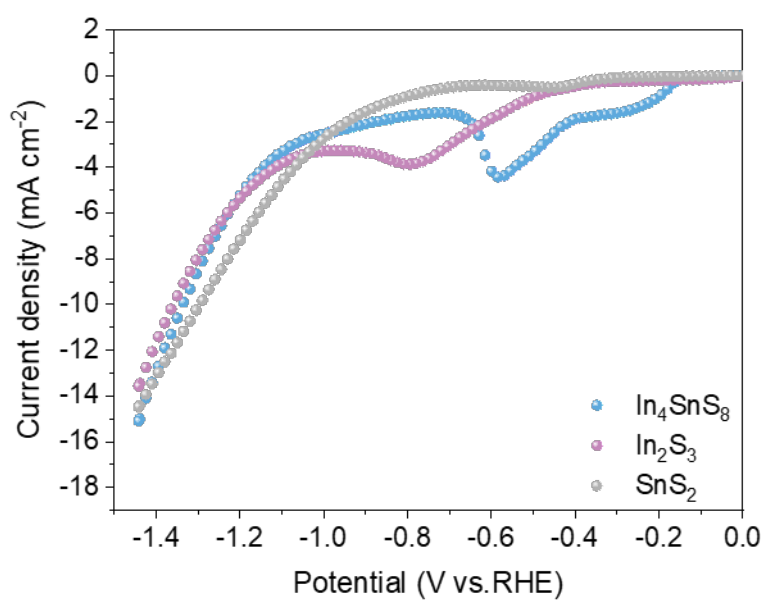


**Fig. S7** LSV curves of In<sub>4</sub>SnS<sub>8</sub>, In<sub>2</sub>S<sub>3</sub>, SnS<sub>2</sub> in 0.1 M KNO<sub>3</sub> electrolyte with CO<sub>2</sub>.



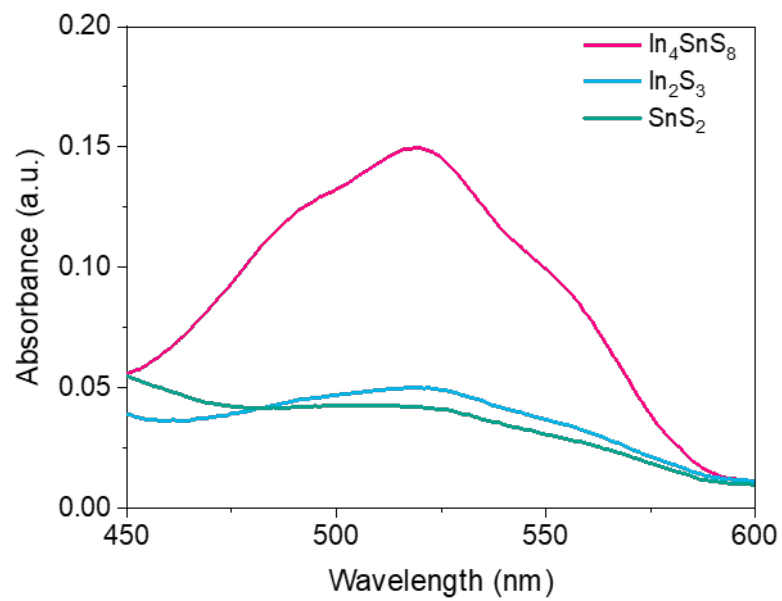


**Fig. S8** UV-vis absorption spectra of urea formed by  $\text{In}_4\text{SnS}_8$ ,  $\text{In}_2\text{S}_3$ ,  $\text{SnS}_2$  at  $-0.65$  V(vs.RHE).

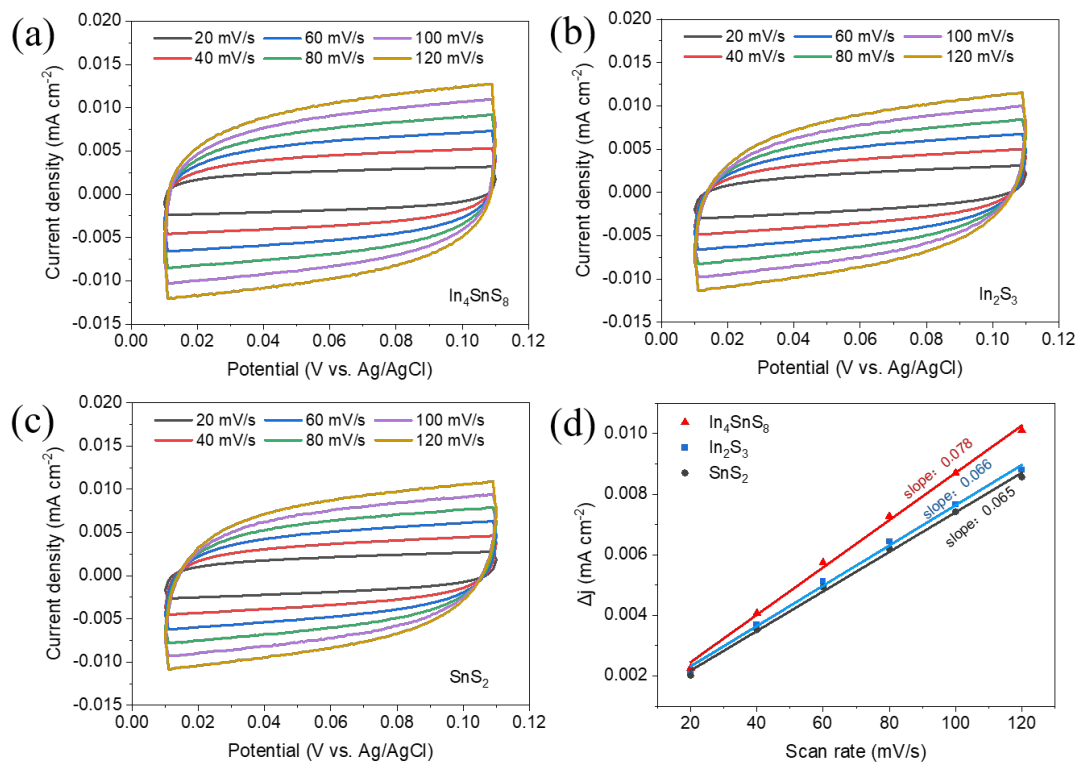


**Fig. S9** Cyclic voltammograms diagrams at different scan rates of (a)  $\text{In}_4\text{SnS}_8$ ; (b)  $\text{In}_2\text{S}_3$ ; (c)  $\text{SnS}_2$ ; (d) Functional relationship of different scanning speeds and current density.

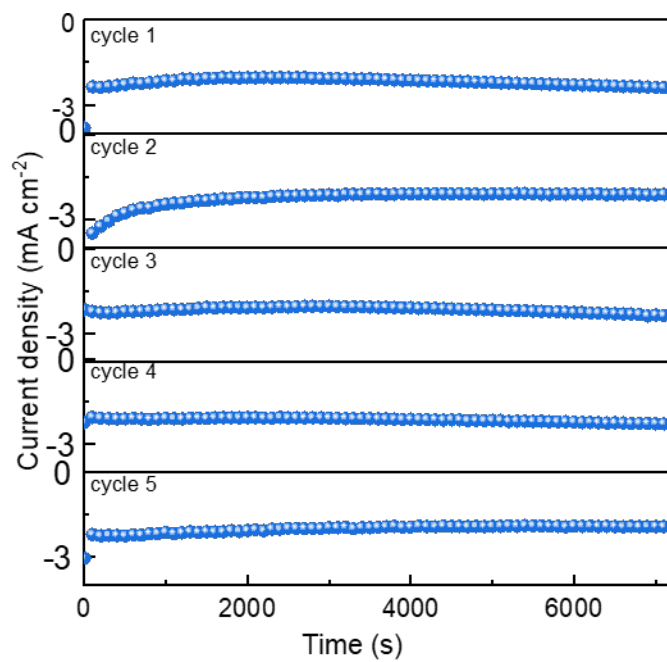


**Fig. S10** The chronoamperometric curves in the five-cycle test over In<sub>4</sub>SnS<sub>8</sub>.

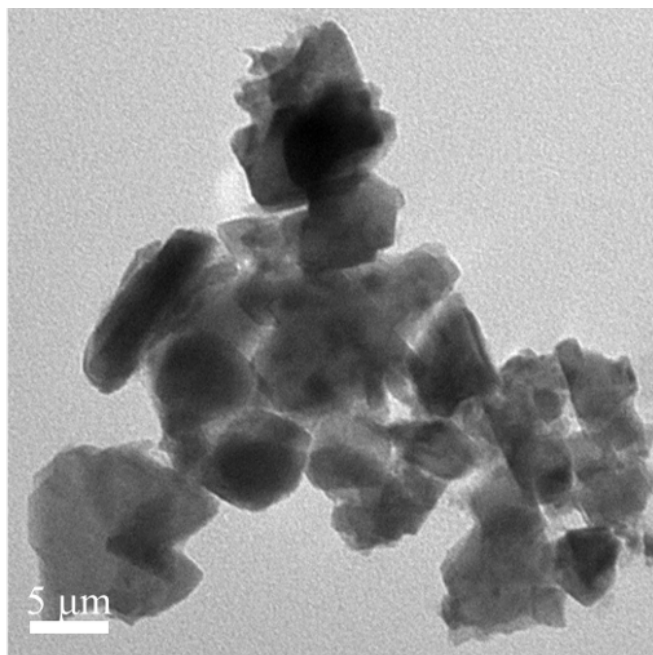


**Fig. S11** TEM image of In<sub>4</sub>SnS<sub>8</sub> after 2 h reaction.

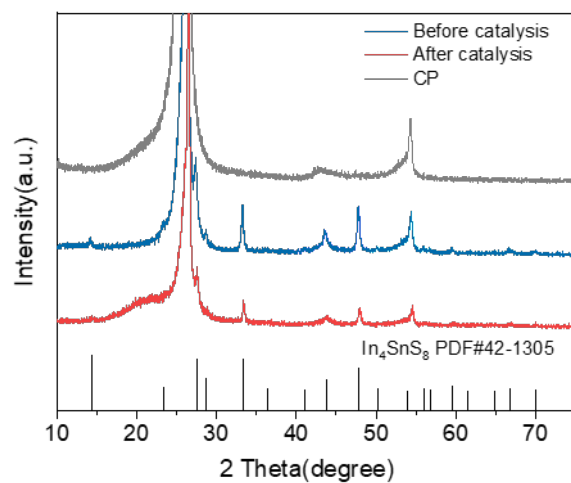


**Fig. S12** XRD pattern of  $\text{In}_4\text{SnS}_8$  after 2 h reaction.

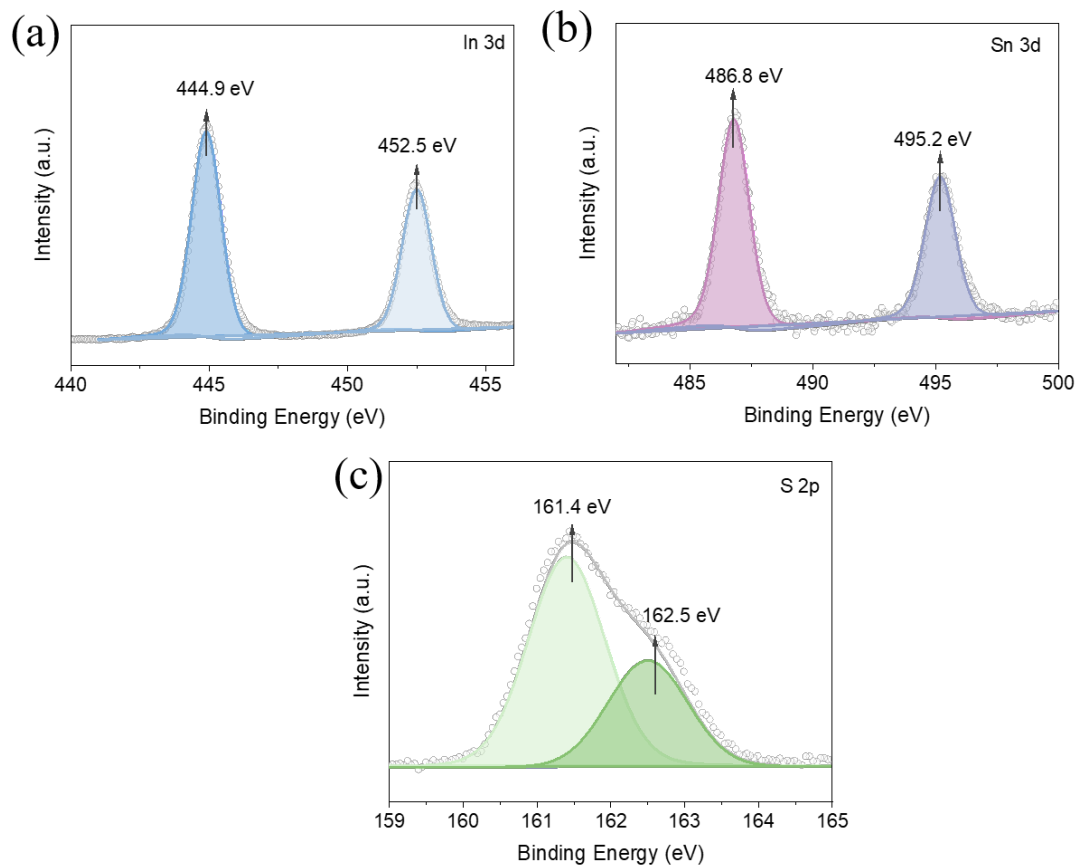


**Fig. S13** (a) In 3d;(b) Sn 3d and (c) S 2p spectrum of  $\text{In}_4\text{SnS}_8$  after 2 h reaction.

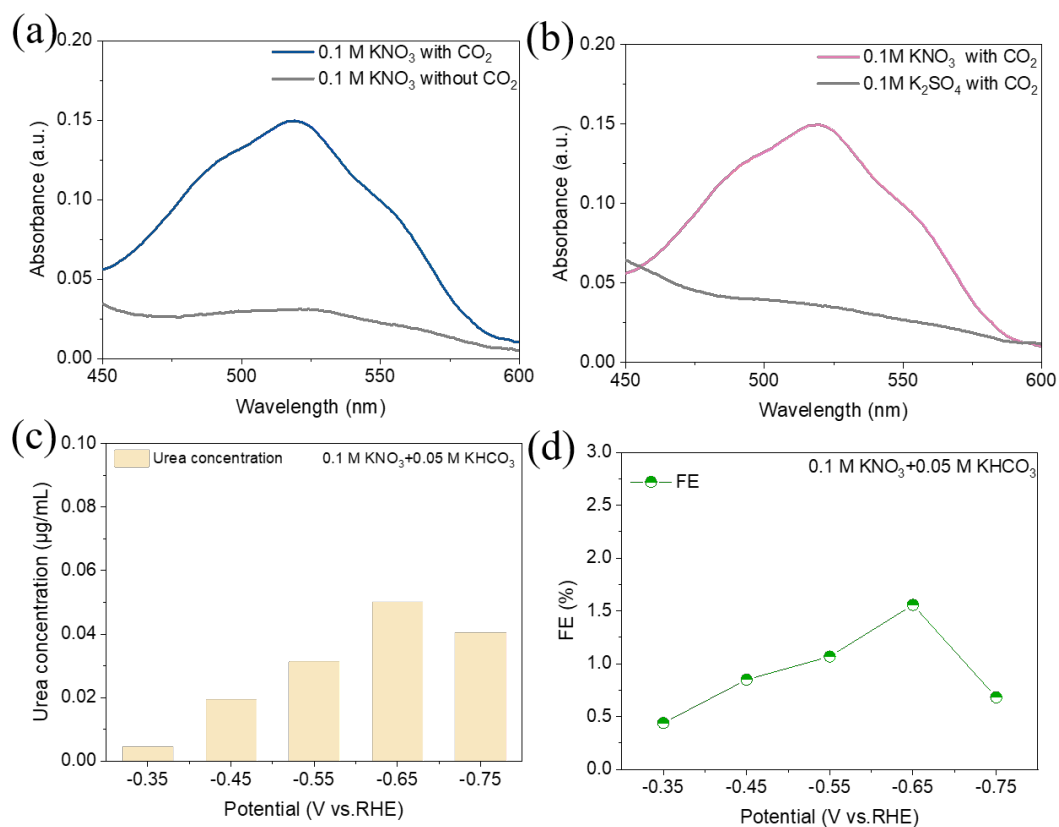


**Fig. S14** UV-vis absorption spectra of (a) 0.1 M  $\text{KNO}_3$  with and without  $\text{CO}_2$  over  $\text{In}_4\text{SnS}_8$  after 2 h reaction at -0.65 V versus RHE; (b) 0.1 M  $\text{K}_2\text{SO}_4$  with and without  $\text{CO}_2$  over  $\text{In}_4\text{SnS}_8$  after 2 h reaction at -0.65 V versus RHE; Electrocatalytic performance of urea synthesis over  $\text{In}_4\text{SnS}_8$  at different potentials in 0.1 M  $\text{KNO}_3$  + 0.05 M  $\text{KHCO}_3$  electrolyte without  $\text{CO}_2$ : (c) Urea concentration (d) Faraday efficiency.

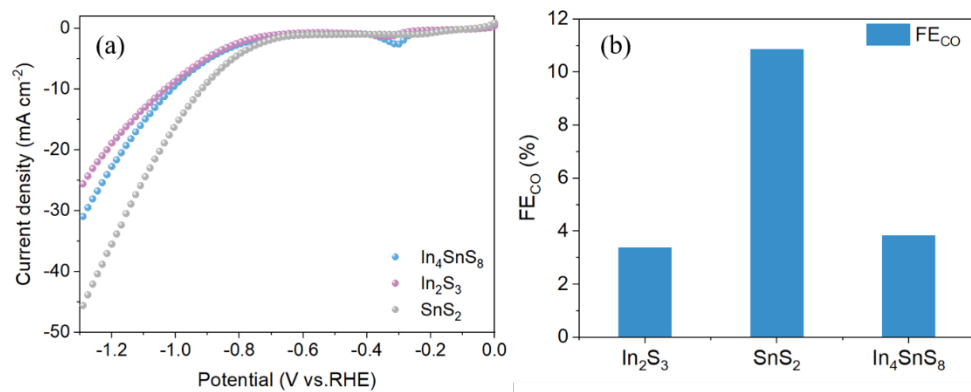


**Fig. S15** (a) LSV curves of In<sub>4</sub>SnS<sub>8</sub>, In<sub>2</sub>S<sub>3</sub> and SnS<sub>2</sub> in 0.1 M KHCO<sub>3</sub> electrolyte with CO<sub>2</sub>; (b) Faradaic efficiency of CO for In<sub>4</sub>SnS<sub>8</sub>, In<sub>2</sub>S<sub>3</sub> and SnS<sub>2</sub> at -1.0 V (vs.RHE).



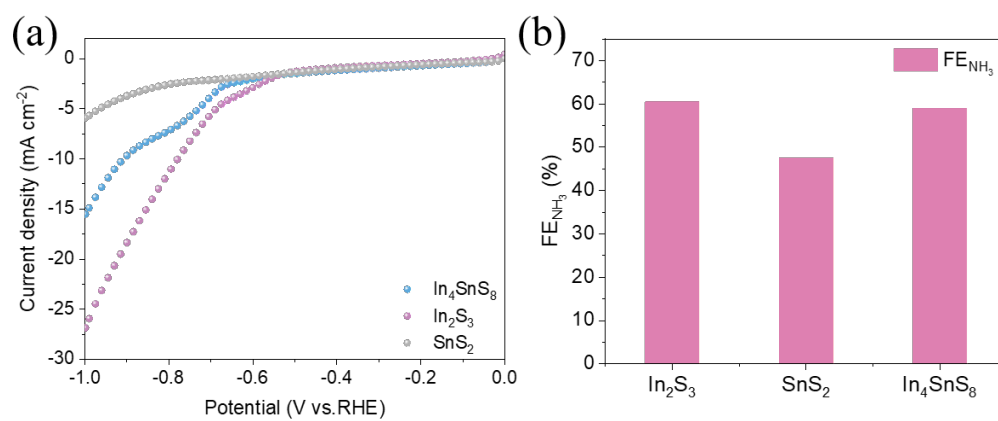


**Fig. S16** (a) LSV curves of In<sub>4</sub>SnS<sub>8</sub>, In<sub>2</sub>S<sub>3</sub> and SnS<sub>2</sub> in 0.1 M KNO<sub>3</sub> electrolyte; (b) Faradaic efficiency of NH<sub>3</sub> for In<sub>4</sub>SnS<sub>8</sub>, In<sub>2</sub>S<sub>3</sub> and SnS<sub>2</sub> at -1.0 V(vs.RHE).

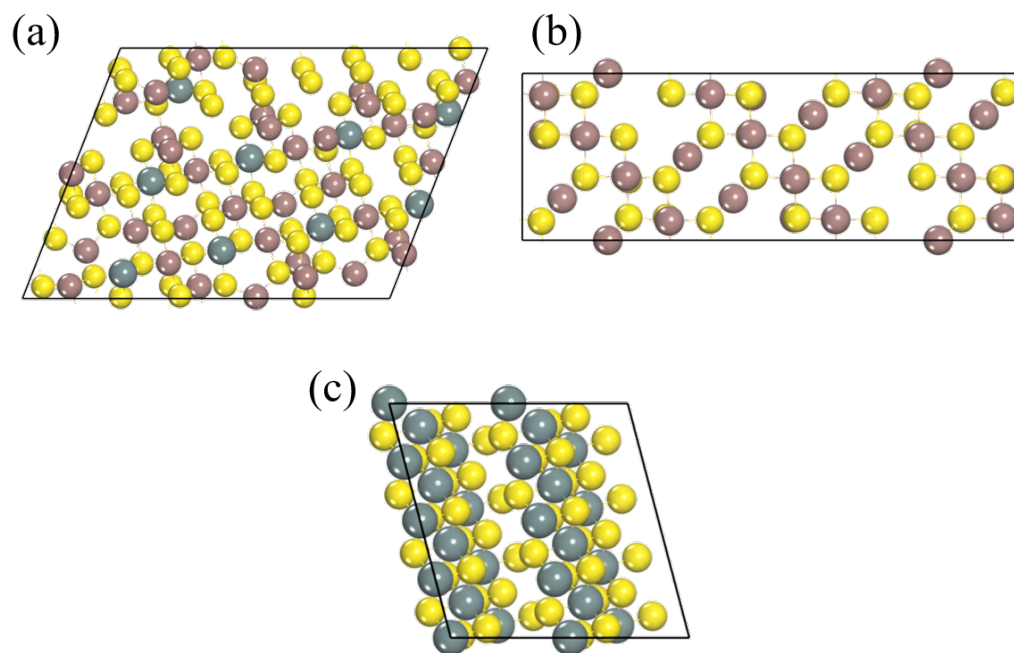


**Fig. S17** DFT calculation models of (a)  $\text{In}_4\text{SnS}_8$ ; (b)  $\text{In}_2\text{S}_3$ ; (c)  $\text{SnS}_2$ .

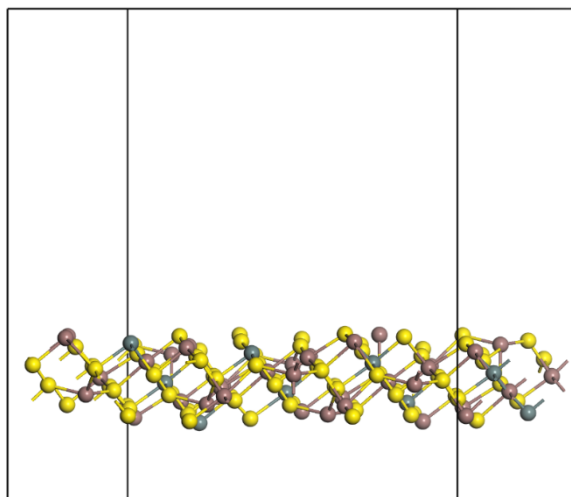


**Fig. S18** The side view of the In<sub>4</sub>SnS<sub>8</sub>(311) surface.

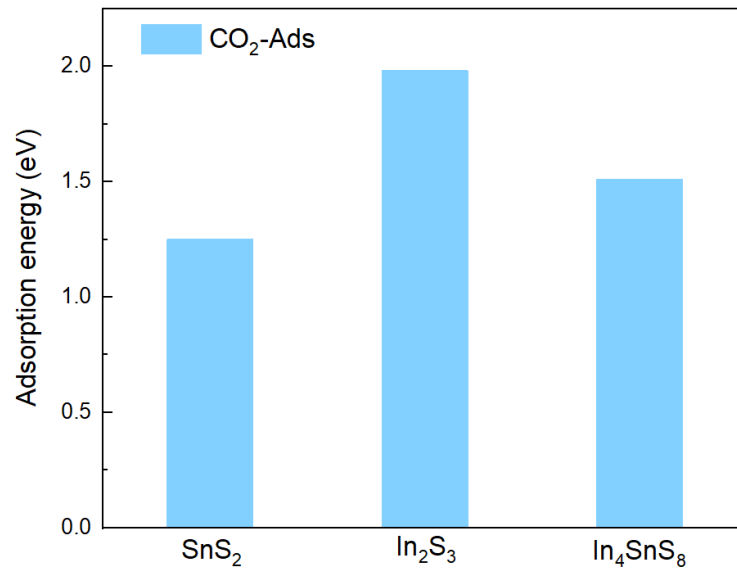


**Fig. S19** The adsorption energy of CO<sub>2</sub> on SnS<sub>2</sub>(101), In<sub>2</sub>S<sub>3</sub>(440) and In<sub>4</sub>SnS<sub>8</sub>(311) surface.

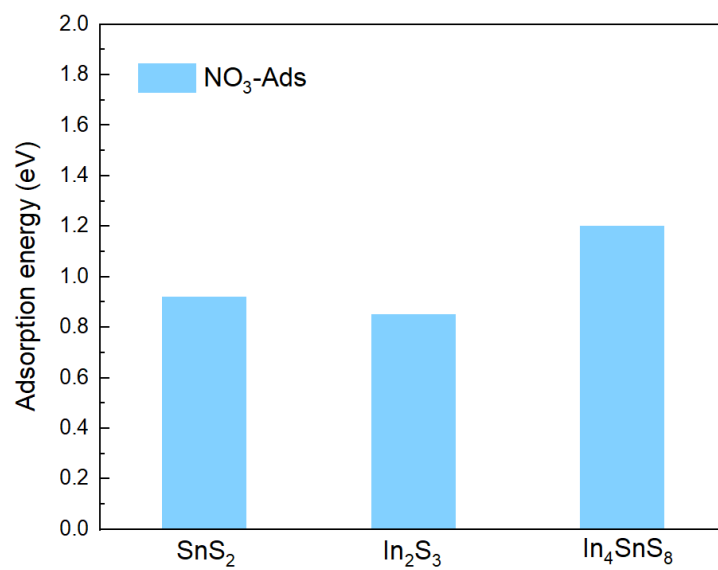


**Fig. S20** The adsorption energy of nitrate on SnS<sub>2</sub>(101), In<sub>2</sub>S<sub>3</sub>(440) and In<sub>4</sub>SnS<sub>8</sub>(311) surface.

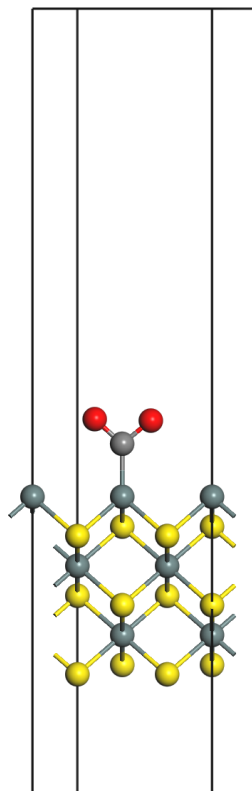


**Fig. S21** The CO<sub>2</sub> adsorption model on SnS<sub>2</sub>(101) surface.

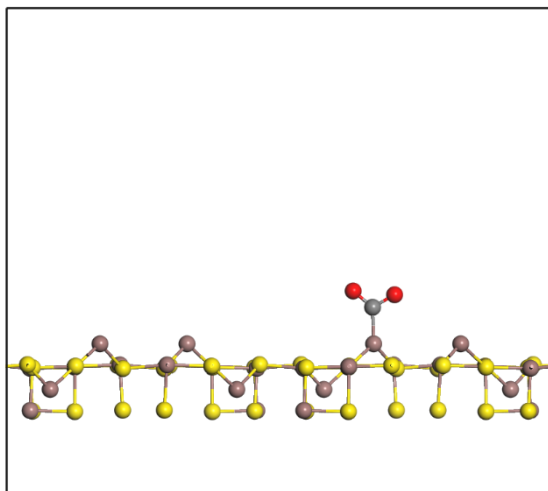


**Fig. S22** The CO<sub>2</sub> adsorption model on In<sub>2</sub>S<sub>3</sub>(440) surface.

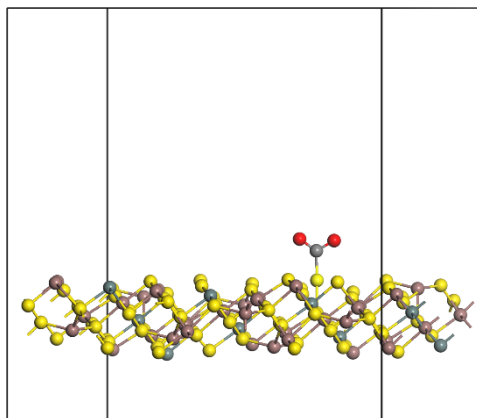


**Fig. S23** The CO<sub>2</sub> adsorption model on In<sub>4</sub>SnS<sub>8</sub>(311) surface.



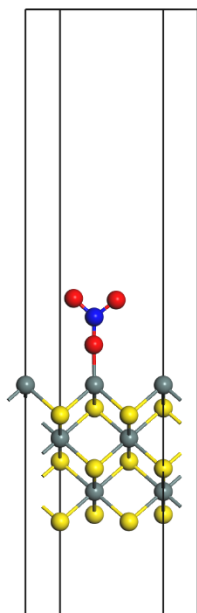


**Fig. S24** The nitrate adsorption model on SnS<sub>2</sub>(101) surface.

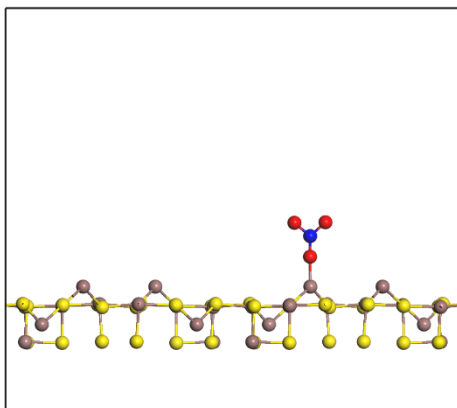


**Fig. S25** The nitrate adsorption model on  $\text{In}_2\text{S}_3(440)$  surface.

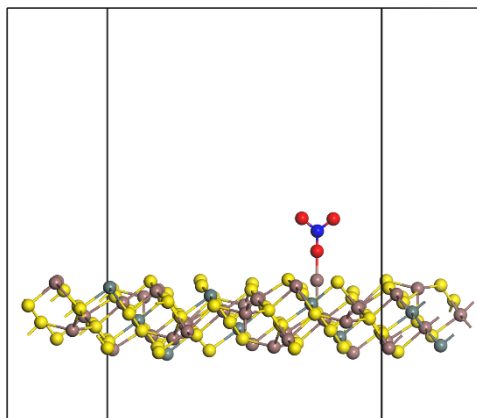


**Fig. S26** The nitrate adsorption model on  $\text{In}_4\text{SnS}_8(311)$  surface.

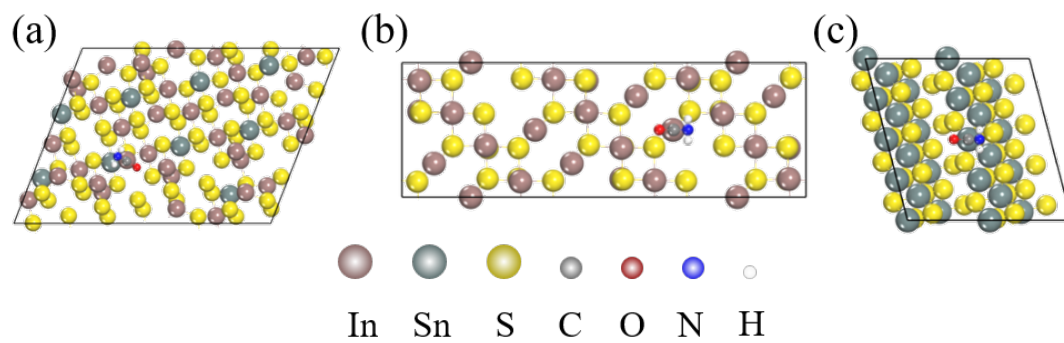


**Fig. S27** DFT calculation models of \*CONH<sub>2</sub> intermediate on the (a) In<sub>4</sub>SnS<sub>8</sub>(311), (b) In<sub>2</sub>S<sub>3</sub>(440) and (c) SnS<sub>2</sub>(101) surface, respectively.